




High mobility Ti, Zr and Ga-codoping In_2O_3 transparent conductive oxide films prepared at low temperatures

Yiyang Liu^{1,2}, Fanying Meng^{1,2,*} , Jianhua Shi¹, Wei Huang^{1,2}, Wenzhu Liu¹, and Zhengxin Liu^{1,2}

¹ Research Center for New Energy Technology (RCNET), Shanghai Institute of Microsystem and Information Technology (SIMIT), Chinese Academy of Sciences (CAS), Jiading, Shanghai 201800, People's Republic of China

² College of Materials Science and Opto-Electronic Technology, University of Chinese Academy of Sciences (UCAS), Shijingshan, 100049 Beijing, People's Republic of China

Received: 25 September 2020

Accepted: 7 December 2020

Published online:

27 January 2021

© The Author(s), under exclusive licence to Springer Science+Business Media, LLC part of Springer Nature 2021

ABSTRACT

High mobility transparent conductive Zr, Ti and Ga-doped indium oxide (ITGZO) films were deposited by radio frequency (RF) magnetron sputtering method at the low deposition temperature. The effects of deposition temperatures on structural, electrical, and optical properties of ITGZO films were investigated in this work. High mobility of $94 \text{ cm}^2/\text{V S}$ was achieved at the deposition temperature of 70°C along with the annealing process. Furthermore, the optical transmittance of ITGZO films has increased by 18% at the infrared wavelength region from 1500 to 2580 nm; compared to the typical Sn-doped indium oxide (ITO) films, this excellent transmittance is mainly attributed to the less free carrier absorption (FCA) thanks to the low carrier concentration of less than $2.0 \times 10^{20} \text{ cm}^{-3}$. In addition, the surface morphology of ITGZO films demonstrated that Ga element would precipitate on the film surface when oxygen was insufficient during the film growth, which indicates that Ga element exists as an oxidation state rather than interstitial atom in ITGZO films; correspondingly, the impurity ion scattering of carriers would be effectively suppressed, which accounts for the high mobility of ITGZO films. Moreover, ITGZO film shows a very low extinction coefficient (k) of 10^{-4} at 633 nm after annealing, which implies almost zero absorption loss from ITGZO films. Based on the higher mobility and better optical properties, it is expected that ITGZO film is a promising alternative material substituting for the typical ITO film in the advanced optoelectronic devices.

Address correspondence to E-mail: fymeng@mail.sim.ac.cn

1 Introduction

Transparent conducting oxides (TCO) have been widely used in many fields including organic light-emitting panel display, transparent field effect transistor and solar cells [1]. In particular, the In_2O_3 -based thin films have attracted considerable attention due to their excellent electrical properties [2]. Such as the application of silicon heterojunction solar cells [3, 4], the use of ITO [5] greatly compensates for the poor lateral conductivity of hydrogenated amorphous silicon, thereby significantly improving the carrier collection efficiency. However, the relatively high carrier concentration in ITO affects the transmittance of the film at the infrared wavelength region due to the FCA effect, which is one of the factors limiting the efficiency of silicon heterojunction solar cells. Therefore, it is of great significance to develop new TCO materials with superior transmittance and low carrier concentration. Besides, ITO has gradually become an excellent tunable material for active photonic devices in recent years due to its high electron mobility and extremely low dielectric constant [6]. The transparent and conductive properties of ITO also make it a supporting material for the metal–organic frameworks to assist research [7]. In the field of photocatalyst research, indium oxide can be used as a participating material to improve the production of photocatalytic hydrogen [8]. Also, indium oxide can modify the glassy carbon electrode to obtain good electrochemical performance [9].

To optimize the optical transmittance of TCO without sacrificing electrical conductivity, metal doping has proved to be an effective approach [10–12]. Among the numerous dopants, Ti and Zr doping has been proved to increase the visible and near-infrared transmittance of thin films while maintaining high mobility [13–15]. W [2] and Mo doping can significantly improve the work function, thus effectively reducing the mismatch loss between TCO and certain semiconductors. The deposition temperature is also one of the key parameters to determine TCO film's performance, and appropriate heating can help modify the photoelectric properties of TCO films [16, 17]. In various deposition methods, RF magnetron sputtering [18, 19] is feasible to achieve industrialization; meanwhile, TCO made by this technology has the advantages of good uniformity and high density.

In this work, Ti, Zr and Ga factors were used as dopants in In_2O_3 -based material to enhance its electronic transmission and optical window characteristics. ITGZO films were fabricated via RF magnetron sputtering method. The structural, electrical, and optical properties of ITGZO films at various deposition temperatures after annealing were investigated in detail. It was discovered that compared with the conventional ITO films, our ITGZO films exhibit more excellent mobility and higher infrared wavelength region transmittance, which have great potential for the application of optoelectronic devices such as solar cells. Moreover, in other TCO application area such as communication, device processing may undergo high-temperature steps; hence, we also annealed ITGZO films at 350 °C and analyzed its photoelectric properties.

2 Experimental

ITGZO film was deposited on $5 \times 5 \text{ cm}^2$ glass (Corning7059) by RF magnetron sputtering. The glass was ultrasonically cleaned by acetone, alcohol and deionized water for 15 min, followed by dried with a nitrogen gun. The source material was a 6-inch ceramic target with a doping ratio of $\text{IO}:\text{ZrO}_2:\text{TiO}_2:\text{Ga}_2\text{O}_3$ equal to 98.5:0.5:0.5:0.5. The angle between the pallet and the target plane was 30°, and the distance from the center of the pallet to the target is 110 mm. The substrate temperature during the film deposition process were 25 °C (room temperature, RT), 70 °C, 115 °C, and 160 °C, respectively. Two heating rods were used for heating the chamber, and three temperature sensors were set for temperature feedback. Before gases entered the chamber, the background pressure was set to $9 \times 10^{-4} \text{ Pa}$, the introduced gases contain argon and oxygen, and the ratio of oxygen/(argon + oxygen) was 0.008. After the gases filled the chamber, we manually adjusted the chamber pressure to 0.45 Pa. The surface of the target was cleaned by pre-sputtering for 15 min; during this process, the metal baffle in front of the target was closed to avoid contaminating the substrate. The sputtering power was set at 120 W, the tray speed was 2000 r/h, and the thickness of the films were kept around 80 nm. Films with the thickness of 350 nm were also prepared for SEM profile analysis. All the samples were annealed at 200 °C for 30 min in air atmosphere. As

an extended study, ITGZO RT samples annealed at 350 °C were also prepared.

Film thickness, n and k were measured via a spectroscopic ellipsometer (SE, J.A. Woollam Co., Inc. M-2000) with the Drude and Tauc–Lorentz model. Hall measurement (Ecopia HMS-5300 system) was used to evaluate the electrical properties including carrier concentration, resistivity and mobility of the films at room temperature with the van der Pauw method. Uv–Vis–NIR spectrometer (Perkin-Elmer Lambda 950) was used to characterize the transmittance and reflectivity at wavelengths of 280–2580 nm of ITGZO films. Rigaku D/max 2200/PC X-ray diffraction (XRD) was used to characterize the crystalline structure of ITGZO films with Cu-K α radiation source ($k = 1.5405 \text{ \AA}$), the diffraction angle ranging from 20° to 70° at 2θ scan mode. The microstructure of ITGZO films were analyzed via scanning electron microscopy (SEM, Merlin Compact) and atomic force microscope (AFM, NT-MDT NTEGRA).

3 Results and discussion

3.1 Structure properties of ITGZO films

Figure 1 shows the XRD spectra of ITGZO films deposited at different deposition temperatures of RT, 70 °C, 115 °C and 160 °C, respectively, after 200 °C annealing. Obviously, our ITGZO films have obvious (222) preferred orientation at 30.6°, and the peak

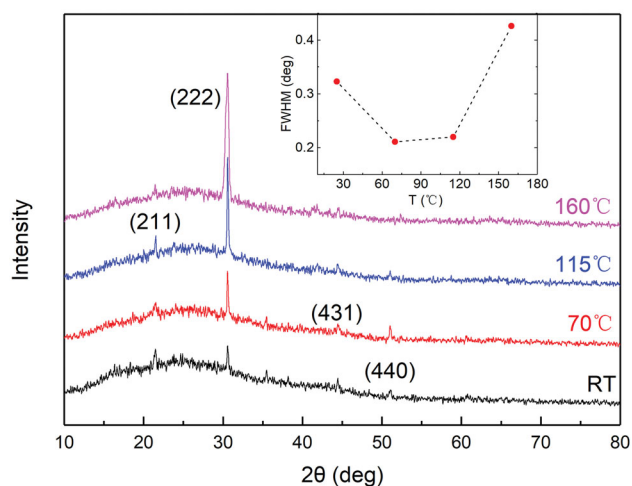
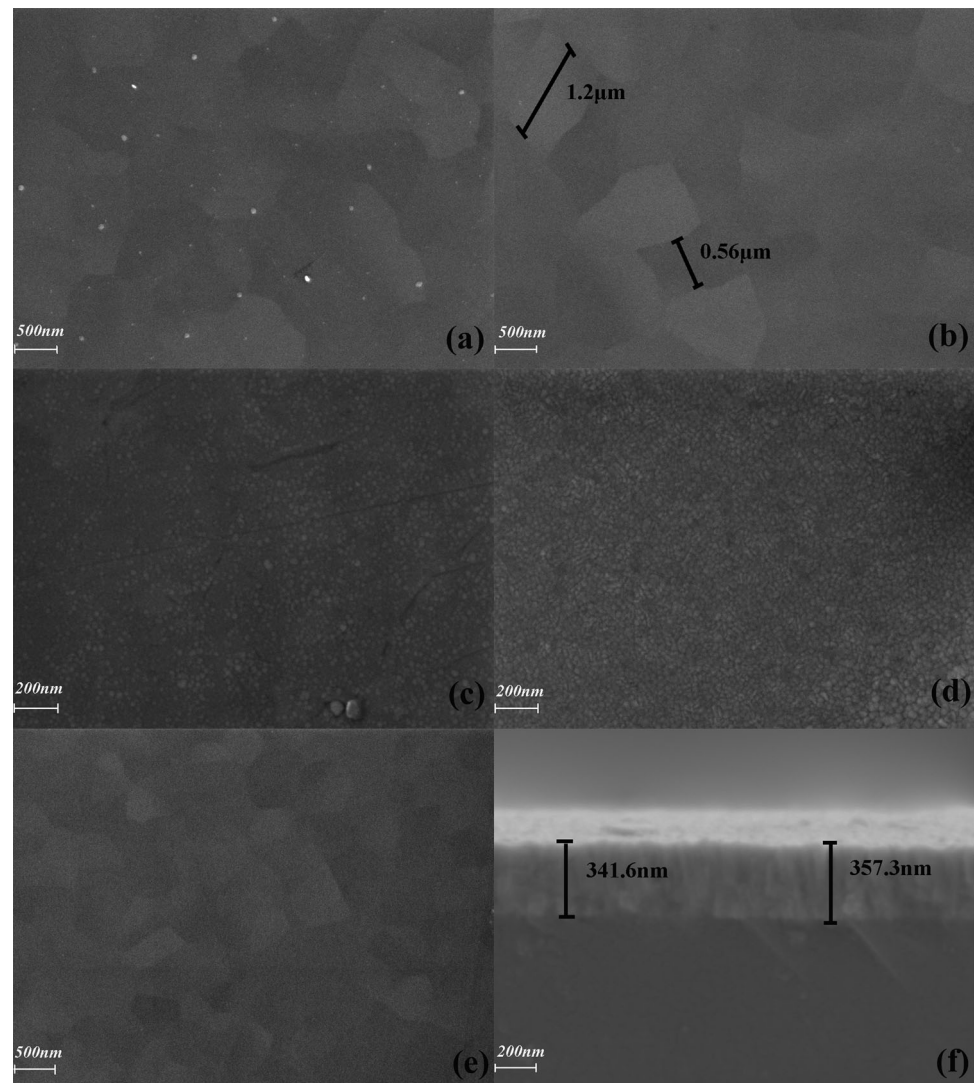


Fig. 1 XRD spectra of ITGZO films deposited at different temperatures of RT, 70 °C, 115 °C and 160 °C, respectively, after 200 °C annealing. The inside set shows the FWHM of peak (222) of ITGZO films

intensity increases with deposition temperature, indicating that high temperature is more conducive to the growth of (222) orientation, several weak peaks of ITGZO films at 21.5°, 44.5°, and 51° can also be checked. The (222), (211) and (440) diffraction peaks of ITGZO films are well matched with the unit cell of a cubic In_2O_3 powder data (JCPDS No. 6–416), indicating that there is no additional phase related to dopants; although the ionic radii of the dopants are different from that of In ions, the doping volume is too small to cause a peak shift. However, the (431) diffraction peaks of ITGZO films are slightly offset by 1.2 degree in the direction of small angle compared with In_2O_3 powder, indicating that there may be lattice distortion caused by residual stress in the ITGZO films. Otherwise, all peak positions of ITGZO films are independent of deposition temperature, confirming that the change of deposition temperature did not cause phase transition. The inside set shows the full width at half maxima (FWHM) of peak (222) at different deposition temperatures, the value of FWHM decreases first and then increases, 70 °C film shows the smallest FWHM value, indicating a larger crystallite size compared with other films.

The surface and cross-section microstructure of ITGZO films after 200 °C annealing were investigated using SEM as shown in Fig. 2. The deposition temperatures of Fig. 2a–d are RT, 70 °C, 115 °C and 160 °C, respectively. Figure 2e shows the surface microstructure of RT-film under higher oxygen partial pressure of 0.02 and Fig. 2f illustrates the cross-section structure of 160 °C film with thicker thickness of 350 nm. From Fig. 2a–d, we can observe three obvious phenomena: firstly, as the temperature increases, a growth mode transition from two-dimensional (2D) to three-dimensional (3D) was discovered, the RT and 70 °C-films were extremely smooth; however, when the deposition temperature reached to 115 °C and 160 °C, the film exhibited a rough surface. Then we used AFM to evaluate the roughness of these ITGZO films, as shown in Fig. 3, in which a–d show the ITGZO films' 3D morphology at different deposition temperatures, and the box plot in Fig. 3e summarizes the relative values of film surface roughness, including peak minimum, maximum, mean, median, upper quartile and lower quartile of film surface. The colored symbols indicate the root mean square (RMS) of the roughness of ITGZO films deposited at different temperatures. The

Fig. 2 SEM images of ITGZO films under different preparation conditions after annealing: **a–d** Deposition temperature are RT, 70 °C, 115 °C and 160 °C, respectively; **e** partial pressure of oxygen increased to 0.02; **f** profile morphology of 350 nm-ITGZO film



RMS of 160 °C film is 1.498 nm, while the RMS of 70 °C film is only 0.432 nm.

Secondly, the grain size of ITGZO films first increases and then decreases with deposition temperature, accompanying a transformation from crystallites to nanocrystals, which is consistent with the FWHM results of XRD. The grain size of 70 °C film can be as large as 1 micron, while the 160 °C film is only tens of nanometers.

Thirdly, a distribution of unintentional nanoscale white particles appeared on RT-ITGZO film surface. We have tried to use energy dispersive spectrometer (EDS) to analyze the composition of these white particles, but the result was not as expected because the size of the white particles were too small to reach the accuracy of the instrument. Therefore, we explain this phenomenon from a theoretical perspective, and

then verify it through experiment. The melting point and boiling point of several doped elements in ITGZO are shown in Table 1.

We can see that the melting and boiling points of In, Zr and Ti elements are very high, while Ga's melting point is 29.8 °C. This is because gallium metal exists in the form of Ga_2 molecules, and its intermolecular force is relatively small, so smaller energy can melt it into a liquid state. However, the gas gallium exists in the form of Ga atoms, and its gasification requires the breaking of the chemical bonds in Ga_2 , so higher energy is required. From the perspective of the metal activity series, Ga element is relatively easy to be reduced, so we speculate that the white particles may be the reduced Ga precipitating on the RT-film surface under the condition of insufficient oxygen. Based on this assumption, when the

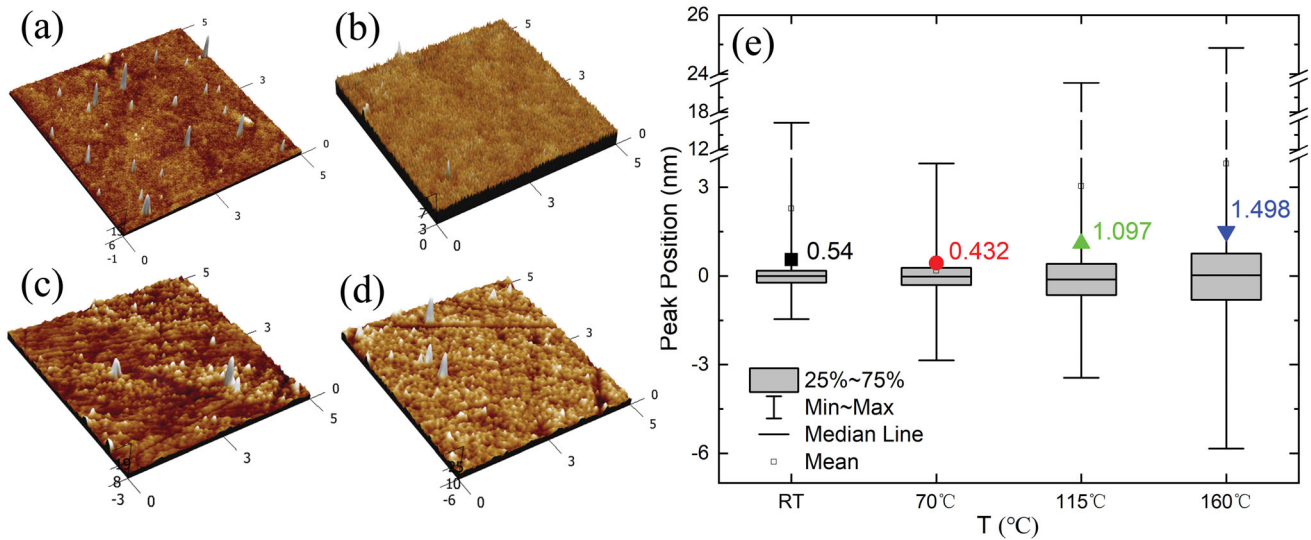


Fig. 3 AFM images of ITGZO thin films: **a–d** Deposition temperatures are RT, 70 °C, 115 °C and 160 °C in sequence; **e** box plot consisting of peak minimum, maximum, mean, median, upper

Table 1 Melting and boiling points of four metal elements in ITGZO

Element	Melting point (°C)	The boiling point (°C)
In	156.61	2060
Zr	1852	4377
Ti	1668	3287
Ga	29.8	2403

deposition temperature higher than Ga's melting point, the reduced Ga also be melted. In addition, the sputtering process will continuously inject kinetic energy into the film surface, excessive energy caused the molten Ga to occur a liquid–vapor phase transition. Eventually, such white particles were observed only on the surface of RT-film. To verify the correctness of this speculation, we increased the oxygen partial pressure to 0.02. The surface morphology of 0.02-RT-film is shown in Fig. 2e, no white particles observed. This result further strengthened the credibility of Ga's reduce process of “precipitation → melting → evaporation” with insufficient oxygen.

3.2 Electric properties of ITGZO films

Table 2 shows the electrical properties of the as-deposited (AS) and 200 °C post-annealing (PA) ITGZO films prepared by various deposition temperatures.

quartile and lower quartile of each film surface, and the colored symbols indicate corresponding RMS values

For comparison, the data of ITO thin film deposited at room temperature are also shown in the table. For AS sample, the carrier concentration of ITGZO film increases first and then decreases with deposition temperature. Appropriate high temperature is beneficial for the substitution reaction of doping cations; the substitution reaction rate reaches its maximum at 115 °C, after which the carrier concentration does not increase anymore, and continued heating will strengthen the energy of the sputtered particles, and then the excessive high energy will destroy the existing lattice structure; even the doping cations that successfully replaced the position of In ions will be knocked out of the lattice, which will paralyze the substitution reaction and reduce the carrier concentration. Post-annealing decreased carrier concentration of all the samples because of the eliminating of oxygen vacancy around air atmosphere.

The mobility of AS-ITGZO films decreases with deposition temperature; however, the fluctuation is not obvious. After annealing, all samples' mobilities increase, and the gap between the samples at different temperatures has become obvious. The mobility of 70 °C film is as high as 93.98 cm²/V·S, which is 44 cm²/V·S more than the corresponding AS sample; this is because annealing caused the films' crystallization, and some oxygen vacancy defects were eliminated under the air atmosphere [20, 21]. High-quality crystal has less grain boundary and impurity ion scattering, thus the mobility improved. The initial

Table 2 Electrical properties of ITGZO films prepared by various deposition temperatures

	Carrier concentration (cm ⁻³)		Resistivity (Ω·cm)		Carrier mobility (cm ² /V·S)	
	AS (× 10 ²⁰)	PA (× 10 ²⁰)	AS (× 10 ⁻⁴)	PA (× 10 ⁻⁴)	AS	PA
RT	3.67	1.79	4.18	3.93	40.84	89.04
70 °C	3.79	1.94	4.10	3.47	40.32	93.98
115 °C	3.82	1.89	4.16	4.07	39.35	81.26
160 °C	2.99	1.72	5.77	5.77	36.64	65.01
ITO	7.16	5.82	6.20	4.10	14.53	26.63

state of 70 °C film has the highest “reforming potential”, so the mobility increased the most after annealing, which is consistent with the SEM characterization results above. However, 200 °C annealing treatment did not improve 160 °C film’s mobility significantly; in order to clarify the reason, we have added the research on the cross-sectional structure of ITGZO films. 80 nm films are too thin to see clearly, so we fabricated thicker films of 350 nm. It is worth noting that a columnar crystal structure appeared in 350 nm–160 °C film as shown in Fig. 2f; this growth mode was not found in other samples. Theoretically, the columnar crystallization method will reduce carrier grain boundary scattering in vertical direction [22], which is conducive to the improvement of vertical mobility. However, Hall test reflects lateral mobility, and the grain boundary scattering in the horizontal direction of columnar crystal may be very serious, so we observed a poor mobility of 160 °C film. Of course, the low mobility may also be due to the poor crystal quality caused by deposition temperature of 160 °C. In the process of film deposition, high temperature is likely to cause the desorption of molecules or atoms that have been adsorbed on the surface of the material, thus leading to a large number of defects in the films, and carriers would be captured by recombination traps at these defects, resulting in low mobility of 160 °C film.

Resistivity affected by both the carrier concentration and the mobility. The formula is expressed as $\rho = 1/\mu N_e q$, where ρ is the resistivity, μ is the mobility, N_e is the carrier concentration, and q is the electric charge of a single electron. AS sample’s resistivity first decreases and then increases with increasing temperature. 70 °C film exhibits the smallest resistivity with a value of $4.10 \times 10^{-4} \Omega \cdot \text{cm}$, and the 160 °C film exhibits the highest resistivity with a value of $5.77 \times 10^{-4} \Omega \cdot \text{cm}$. After annealing, the resistivities of all samples have been improved except 160 °C film, indicating that the deposition

temperature of 160 °C may limit the recrystallization of ITGZO film.

3.3 Optical properties of ITGZO films

Figure 4 shows the transmittance and reflectance spectra of ITGZO films. Fig. 4a represents transmittance in the wavelength region of 280–2580 nm. Fig. 4b represents corresponding reflectance, and the contrast ITO spectra also given in the figure as a gray star symbol. We know that three paths occur when light enters a film: reflection, absorption, and transmission. Transmittance of the ITGZO films in the visible and near-infrared wavelength region increases with the deposition temperature, and the reflectance in this region shows the opposite rule. As the wavelength increases, the trends of the transmittance and reflectance of ITGZO films with temperature gradually reverses. However, the turning point of the two is not at the same wavelength, which may be related to the different absorption intensity of ITGZO film to different wavelengths of light. Figure 4 also shows the optical characteristic of conventional ITO film; obviously, the transmittance of ITGZO film is significantly higher than that of ITO film in infrared wavelength region, which is related to the carrier concentration in TCO films as shown in Table 2; the carrier concentration of ITGZO film is significantly lower than that of ITO film, whether it is annealed or not. However, when the wavelength is less than 1200 nm, the transmittance of ITGZO film is slightly inferior to ITO film. In general, the optical characteristics of ITGZO film are related to many factors such as carrier concentration, impurity concentration, lattice structure, and surface roughness of the film surface [23].

The n and k curves of ITGZO and ITO films are presented in Fig. 5. It is found that ITGZO film has higher n and lower k compared to ITO film, especially in the infrared wavelength region, indicating

Fig. 4 Transmittance (a) and reflectance (b) spectra of ITGZO and ITO films after 200 °C annealing. The contrast ITO spectrum also given in the figure as a gray star symbol

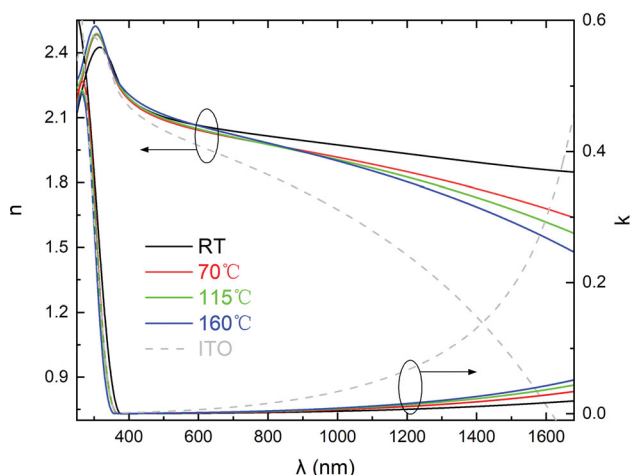
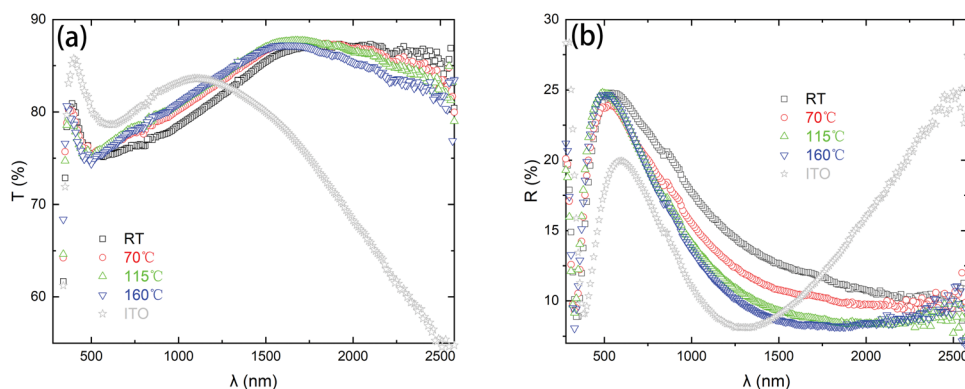


Fig. 5 Refractive index (n) and extinction coefficient(k) curves of ITGZO and ITO films under different deposited temperatures after 200 °C annealing

that ITGZO film has great potential to replace ITO film as an excellent optical window layer material applied on advanced optoelectronic devices. It is worth noting that although the k value of the ITGZO films increases with wavelength, it is still at a relatively low level, even for the 160 °C film.

Fig. 6 Optical bandgap of ITGZO and ITO films at different deposition temperatures after 200 °C annealing; the colorful circle symbols represent ITGZO films and the star symbol represents ITO film deposited at room temperature

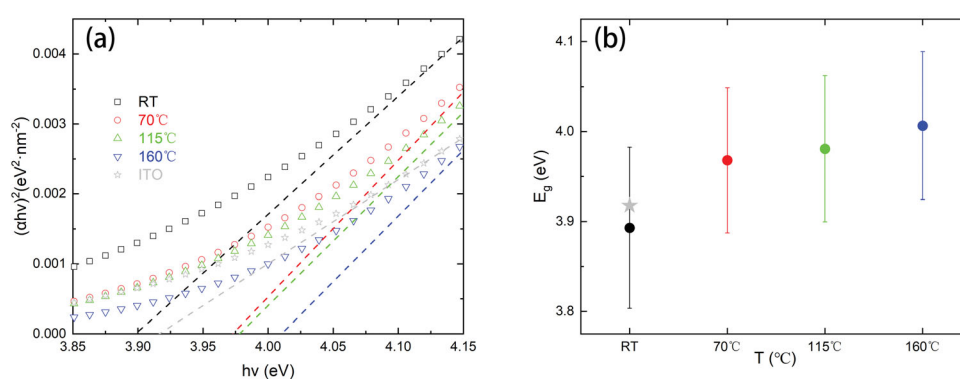


Figure 6 shows the optical bandgap (E_g) of ITGZO and ITO films at different deposition temperatures. By formula [24, 25]:

$$(\alpha h\nu)^2 = A(h\nu - E_g) \quad (1)$$

$$\alpha = \frac{4\pi\kappa}{\lambda} \quad (2)$$

α is the absorption coefficient, h is the Planck constant, ν is the frequency of the incident light, A is a constant, E_g is the forbidden band width, π is the circumference ratio, k is the extinction coefficient, and λ is the wavelength of the incident light. Based on the analysis of optical test results, the $(\alpha h\nu)^2 - h\nu$ curve is shown in Fig. 6a, and the abscissa of the intersection of the tangent and the horizontal axis represents E_g , which is summarized in Fig. 6b. The E_g of ITGZO film increases with the deposition temperature; however, the overall fluctuation is not large, and the values are close to 4 eV. Combining with the above analysis of the microstructure of ITGZO films through XRD and SEM, we found E_g is related to the crystallization of films. Our conclusion is consistent with the result of Yu et al. in the study of nanohydrogenated amorphous silicon (na-Si:H); they believe that the quantum size effect leads to the E_g of na-Si:H

increases with the film crystal ratio (X_c) and the nanograin size (D) decreases [26]. In our study, the film crystal ratio (X_c) increases (shown in Fig. 1 (222) peak enhancement), and the grain size (D) decreases gradually (shown in SEM in Fig. 2) with the increasing of deposition temperature. These changes of crystallization state may be one of the reasons for the increasing of E_g of ITGZO films. In addition, another possible reason is that the deposition temperature affects the cation doping efficiency, leading to different degrees of lattice distortion, and higher deposition temperature may lead to larger atomic spacing, resulting in an increasing of E_g . However, the deeper physical mechanism has not been clarified and require further study.

3.4 Photoelectric performances of high-temperature annealed ITGZO films

The above discussion is based on the 200 °C annealing temperature suitable for some devices with low-temperature process such as silicon heterojunction solar cells. In practice, TCO has wider application scenarios, and higher annealing temperatures may be used in other fields. The Hall measurement results and n , k values at three specific wavelengths of RT-ITGZO films before and after 200 °C and 350 °C annealing are listed in Table 3. Obviously, the annealing process reduced the carrier concentration in ITGZO films, and higher temperature dropped the carrier concentration more seriously, indicating that high temperature is more helpful for the oxygen in the air to occupy the position of the oxygen vacancy in ITGZO films. In the meantime, the participation of oxygen may change the crystalline structure of ITGZO films and thus influence carrier scattering, causing mobility changing. The combined effect of mobility and carrier concentration ultimately resulted a very high resistivity of ITGZO films along with 350 °C annealing process. On the other hand, we found that 350 °C annealing improves the optical properties

of ITGZO films especially in infrared wavelength region. In the application of solar cells, we pay more attention to the wavelengths of 633 nm and 1000 nm; in this article, we also pay attention to the longer wavelength of 1500 nm. From the results, we know that the k of annealed ITGZO is only 10^{-4} at the wavelength of 633 nm; when the annealing temperature is increased from 200 to 350 °C, the k further drops from 9.44×10^{-4} to 3.10×10^{-4} , which indicates a very low absorption. Even at the wavelength of 1500 nm, the annealing temperature of 350 °C can keep k of ITGZO film as low as 4.25×10^{-3} . Therefore, ITGZO films may have great application potential for devices that require both high-temperature processes and low absorption at infrared wavelength region.

4 Conclusion

In this paper, ITGZO thin films were prepared at different deposition temperatures using RF magnetron methods. The effects of deposition temperature on the structure, electrical, and optical properties were analyzed by various material characterization methods, and the related physical mechanisms were explained. ITGZO film with excellent crystal quality showed better electrical characteristics, 70 °C film has the smallest FWHM value, largest grain size and lowest surface roughness, so it exhibited optimal electrical property. Insufficient oxygen caused part of Ga dopant to precipitate on ITGZO film surface; this phenomenon illustrated that the high mobility of ITGZO film may be the less scattering of interstitial impurity ions. Moreover, ITGZO film exhibited superior optical performance in the infrared wavelength region, which is much better than the typical ITO film, and it showed great potential to replace ITO film as optical window layer applied on certain optoelectronic devices. Finally, we discovered that the annealing temperature of 350 °C is more

Table 3 Photoelectric parameters of ITGZO films before and after high-temperature annealing

	AS	200 °C-PA	350 °C-PA
Carrier concentration (cm^{-3})	3.67×10^{20}	1.79×10^{20}	1.59×10^{19}
Resistivity ($\Omega \text{ cm}$)	4.18×10^{-4}	3.93×10^{-4}	2.28×10^{-2}
Carrier mobility ($\text{cm}^2/\text{V S}$)	40.84	89.04	18.30
633 nm (n , k)	2.05, 2.75×10^{-3}	2.05, 9.44×10^{-4}	2.10, 3.10×10^{-4}
1000 nm (n , k)	1.91, 1.16×10^{-2}	1.97, 3.87×10^{-3}	2.05, 1.25×10^{-3}
1500 nm (n , k)	1.67, 4.46×10^{-2}	1.88, 1.38×10^{-2}	2.02, 4.25×10^{-3}

beneficial to reduce the absorption of ITGZO film around 1500 nm wavelength.

Acknowledgements

This work was partly supported by the Strategic Priority Research Program of Chinese academy of Sciences (XDA17020403), the projects of Science and Technology Commission of Shanghai (17DZ1201100) and (19DZ1207602).

References

1. K. Ellmer, Past achievements and future challenges in the development of optically transparent electrodes. *Nat. Photonics* **6**, 809–817 (2012). <https://doi.org/10.1038/NPHOTON.2012.282>
2. W. Huang, J. Shi, Y. Liu, F. Meng, Z. Liu, Effect of crystalline structure on optical and electrical properties of IWOH films fabricated by low-damage reactive plasma deposition at room temperature. *J. Alloys Compd.* (2020). <https://doi.org/10.1016/j.jallcom.2020.155151>
3. O. Sanchez-Sobrado, M.J. Mendes, T. Mateus, J. Costa, D. Nunes, H. Aguas, E. Fortunato, R. Martins, Photonic-structured TCO front contacts yielding optical and electrically enhanced thin-film solar cells. *Sol. Energy* **196**, 92–98 (2020). <https://doi.org/10.1016/j.solener.2019.11.051>
4. F. Meng, J. Liu, L. Shen, J. Shi, A. Han, L. Zhang, Y. Liu, J. Yu, J. Zhang, R. Zhou, Z. Liu, High-quality industrial n-type silicon wafers with an efficiency of over 23% for Si heterojunction solar cells. *Front. Energy* **11**, 78–84 (2017). <https://doi.org/10.1007/s11708-016-0435-5>
5. D. Wan, P. Chen, J. Liang, S. Liang, F. Huang, (211)-Orientation preference of transparent conducting In_2O_3 : Sn films and its formation mechanism. *ACS Appl. Mater. Interfaces* **3**, 4751–4755 (2011). <https://doi.org/10.1021/am2012432>
6. E. Li, A.X. Wang, Femto-Joule all-optical switching using epsilon-near-zero high-mobility conductive oxide. *IEEE J. Sel. Top. Quantum Electron.* **27**, 1–9 (2021). <https://doi.org/10.1109/JSTQE.2020.3018104>
7. G. Genesio, J. Maynadié, M. Carboni, D. Meyera, Recent status on MOF thin films on transparent conductive oxides substrates (ITO or FTO). *New. J. Chem.* **42**, 2351–2363 (2018). <https://doi.org/10.1039/C7NJ03171H>
8. Y. Chao, P. Zhou, N. Li, J. Lai, Y. Yang, Y. Zhang, Y. Tang, W. Yang, Y. Du, D. Su, Y. Tan, S. Guo, Ultrathin visible-light-driven Mo incorporating In_2O_3 - ZnIn_2Se_4 Z-scheme nanosheet photocatalysts. *Adv. Mater.* (2019). <https://doi.org/10.1002/adma.201807226>
9. C. Sengottaiyan, R. Jayavel, R.G. Shrestha, T. Subramani, S. Maji, J.H. Kim, J.P. Hill, K. Ariga, L.K. Shrestha, Indium oxide/carbon nanotube/reduced graphene oxide ternary nanocomposite with enhanced electrochemical supercapacitance. *Bull. Chem. Soc. Jpn.* **92**, 521–528 (2019). <https://doi.org/10.1246/bcsj.20180338>
10. Z. Zhou, Y. Zhang, X. Chen, S. Li, Y. Zhao, X. Zhang, Innovative wide-spectrum Mg and Ga-Co doped ZnO transparent conductive films grown via reactive plasma deposition for Si heterojunction solar cells. *ACS Appl. Energy Mater.* **3**, 1574–1584 (2020). <https://doi.org/10.1021/acsaelm.9b02064>
11. O. Jung-Woo, O. Hyung-Seok, K. Dong-Joo, S. Youl-Moon, K. Sang-Heum, Effects of titanium doping concentration on the structural and electrical properties of sputtered indium oxide films. *J. Nanosci. Nanotechnol.* **15**, 1525–1528 (2015). <https://doi.org/10.1166/jnn.2015.9337>
12. Y. Li, W. Wang, J. Zhang, R. Wang, Preparation and properties of tungsten-doped indium oxide thin films. *Rare Met.* **31**, 158–163 (2012). <https://doi.org/10.1007/s12598-012-0483-x>
13. T. Koida, M. Kondo, Comparative studies of transparent conductive Ti-, Zr-, and Sn-doped In_2O_3 using a combinatorial approach. *J. Appl. Phys.* (2007). <https://doi.org/10.1063/1.2712161>
14. T. Koida, M. Kondo, High-mobility transparent conductive Zr-doped In_2O_3 . *Appl. Phys. Lett.* (2006). <https://doi.org/10.1063/1.2337281>
15. T. Koida, M. Kondo, Improved near-infrared transparency in sputtered In_2O_3 -based transparent conductive oxide thin films by Zr-doping. *J. Appl. Phys.* (2007). <https://doi.org/10.1063/1.2711768>
16. L.T. Yan, R.E.I. Schropp, Changes in the structural and electrical properties of vacuum post-annealed tungsten- and titanium-doped indium oxide films deposited by radio frequency magnetron sputtering. *Thin Solid Films* **520**, 2096–2101 (2012). <https://doi.org/10.1016/j.tsf.2011.08.060>
17. Y. Tao, B. Zhu, Y. Yang, J. Wu, X. Shi, The structural, electrical, and optical properties of SnO_2 films prepared by reactive magnetron sputtering: influence of substrate temperature and O_2 flow rate. *Mater. Chem. Phys.* (2020). <https://doi.org/10.1016/j.matchemphys.2020.123129>
18. U. Prakash, M.J. Maxwell, G. Kiran, A. Dipendra, R.G. Corey, J.P. Nikolas, Spectroscopic ellipsometry determination of optical and electrical properties of aluminum doped zinc oxide. *Appl. Surf. Sci.* **421**, 852–858 (2017). <https://doi.org/10.1016/j.apsusc.2017.01.139>
19. M. Berginc, A. Čampa, K. Vojisljević, B. Malič, P. Panjan, M. Topič, Relation between sputtering parameters and optical and electrical properties of Ga doped ITO transparent

- conductive oxide. *Energy Procedia* **84**, 183–189 (2015). <https://doi.org/10.1016/j.egypro.2015.12.312>
20. K. Kato, H. Omoto, T. Tomioka, A. Takamatsu, Changes in electrical and structural properties of indium oxide thin films through post-deposition annealing. *Thin Solid Films* **520**, 110–116 (2011). <https://doi.org/10.1016/j.tsf.2011.06.061>
 21. K. Sun, W. Zhou, X. Tang, Z. Huang, F. Luo, D. Zhu, Effects of air annealing on the structure, resistivity, infrared emissivity and transmission of indium tin oxide films. *Surf. Coat. Technol.* **206**, 4095–4098 (2012). <https://doi.org/10.1016/j.surfcoat.2012.04.001>
 22. Y. Lan, Y. Chen, J. He, J. Chang, Microstructural characterization of high-quality indium tin oxide films deposited by thermionically enhanced magnetron sputtering at low temperature. *Vacuum* **107**, 56–61 (2014). <https://doi.org/10.1016/j.vacuum.2014.03.018>
 23. J. Shi, L. Shen, F. Meng, Z. Liu, Structural, electrical and optical properties of highly crystalline indium tin oxide films fabricated by RPD at room temperature. *Mater. Lett.* **182**, 32–35 (2016). <https://doi.org/10.1016/j.matlet.2016.06.084>
 24. D. Jiang, J. Qin, X. Wang, S. Gao, Q. Liang, J. Zhao, Optical properties of NiO thin films fabricated by electron beam evaporation. *Vacuum* **86**, 1083–1086 (2012). <https://doi.org/10.1016/j.vacuum.2011.10.003>
 25. D. Jiang, J. Zhang, Y. Lu, K. Liu, D. Zhao, Z. Zhang, D. Shen, X. Fan, Ultraviolet Schottky detector based on epitaxial ZnO thin film. *Solid-State Electron.* **52**, 679–682 (2008). <https://doi.org/10.1016/j.sse.2007.10.040>
 26. H. Yu, R. Cui, H. Wang, H. Yang, B. Zhao, Z. Zhao, D. Tang, S. Lin, F. Meng, Study of hydrogenated nanoamorphous silicon (na-Si:H) thin film prepared by RF magnetron sputtering for graded optical band gap (E_g^{opt}). *J. Mater. Sci.* **40**, 1367–1370 (2005). <https://doi.org/10.1007/s10853-005-0567-1>

Publisher's Note Springer Nature remains neutral with regard to jurisdictional claims in published maps and institutional affiliations.